

MIT Open Access Articles

Planet matching and orbit determination in multi-planet systems for exoplanet direct imaging

The MIT Faculty has made this article openly available. **Please share** how this access benefits you. Your story matters.

Citation: Morgan, Rhonda M, Vlahakis, Sophia K, Pogorelyuk, Leonid, Grubner, Jennifer N, Fitzgerald, Riley et al. 2021. "Planet matching and orbit determination in multi-planet systems for exoplanet direct imaging." Techniques and Instrumentation for Detection of Exoplanets X, 11823.

As Published: 10.1117/12.2594998

Publisher: SPIE-Intl Soc Optical Eng

Persistent URL: <https://hdl.handle.net/1721.1/145292>

Version: Final published version: final published article, as it appeared in a journal, conference proceedings, or other formally published context

Terms of Use: Article is made available in accordance with the publisher's policy and may be subject to US copyright law. Please refer to the publisher's site for terms of use.



PROCEEDINGS OF SPIE

SPIDigitalLibrary.org/conference-proceedings-of-spie

Planet matching and orbit determination in multi-planet systems for exoplanet direct imaging

Rhonda Morgan, Sophia Vlahakis, Leonid Pogorelyuk, Jenny Gubner, Riley Fitzgerald, et al.

Rhonda Morgan, Sophia K. Vlahakis, Leonid Pogorelyuk, Jenny Gubner, Riley Fitzgerald, Sophia Wang, Kerri Cahoy, "Planet matching and orbit determination in multi-planet systems for exoplanet direct imaging," Proc. SPIE 11823, Techniques and Instrumentation for Detection of Exoplanets X, 118230F (3 September 2021); doi: 10.1117/12.2594998

SPIE.

Event: SPIE Optical Engineering + Applications, 2021, San Diego, California, United States

Planet matching and orbit determination in multi-planet systems for exoplanet direct imaging

Rhonda Morgan^a, Sophia K. Vlahakis^b, Leonid Pogorelyuk^b, Riley Fitzgerald^c, Jenny Gubner^b, Sophia Wang^b, and Kerri Cahoy^b

^aJet Propulsion Laboratory, California Institute of Technology, 4800 Oak Grove Dr., Pasadena, CA, 91109, USA

^bDepartment of Aeronautics and Astronautics, Massachusetts Institute of Technology, 77 Massachusetts Avenue, Cambridge, MA 02139, USA

^cKevin T. Crofton Department of Aerospace and Ocean Engineering, Virginia Polytechnic Institute and State University, 460 Old Turner St., Blacksburg, VA 24061, USA

ABSTRACT

A key aspect of the search for Earth-like exoplanets with direct imaging is determining if the exoplanet is in the habitable zone. Future direct imaging mission concepts such as HabEx and LUVOIR require an efficient cadence of observations. Previous work shows that a minimum of three epochs, spanning more than half a period, can determine orbital parameters to 10% for a single, circular orbit. Multi-planet systems may require a different number and cadence of observations. We begin to address the multi-planet minimum observation approach by considering only the astrometric data of exoplanet candidate objects in high contrast images. Existing multi-planet trajectory matching libraries such as “Orbits For The Impatient” (OFTI) currently require users to specify which point sources belong to which planet and assumes that the user has already matched true-positive detections to planets. Additionally, planet matching needs to be considered when assessing the impact of observation scheduling on trajectory estimation accuracy. To address this need for fitting orbits to multiple objects with limited knowledge, we present an approach using a Monte Carlo study of different observation schedules and planetary systems in which we have developed an algorithm to automatically match observations to planets, and then check the accuracy of the matches. With a large number of cases, we can constrain the number of observations and the spacing necessary to “deconfuse” the detections. We present preliminary planet matching success rates for different observing schedules and planetary system parameters. We use these results to assess the scope of the confusion problem and discuss potential mitigation strategies.

Keywords: Exoplanets, multi-planet systems, direct imaging, HabEx, LUVOIR, deconfusion, orbit fitting, starshade, coronagraph

1. INTRODUCTION

The Habitable Exoplanet Observatory (HabEx)¹ and the Large UV/Optical/Infrared Surveyor (LUVOIR)² are two concepts for potential future flagships that would be capable of directly imaging an Earth-like planet in the habitable zone of nearby sun-like stars. The Roman Space Telescope’s Coronagraphic Instrument (CGI) is a technology demonstration that will directly image exoplanets in reflected starlight. Roman CGI will initially image gas giants discovered through radial velocity measurements, while HabEx and LUVOIR would perform blind-search surveys to discover Earth-like planets.

HabEx and LUVOIR have three main goals regarding Earth-like exoplanets: discover them, acquire spectra of them, and determine if they are in the habitable zone. The approach taken by HabEx and LUVOIR in the observing scenario to achieve these goals is to perform the blind search survey in photometric detection to an SNR of 7; then, once a discovery is made, to follow up with additional photometric observations until the orbit is determined sufficiently to know if the planet is in the habitable zone (e.g. the semi-major axis, eccentricity, and

Further author information: (Send correspondence to Rhonda Morgan)
E-mail: rhonda.morgan@jpl.nasa.gov

inclination are known to 10% 1σ error); if the planet is in the habitable zone, then a spectral observation is taken. The spectral observation for HabEx is taken to an SNR of 10 at a spectral resolution of 140 over an instantaneous bandwidth from 300 nm to 1000 nm. The spectral observation for LUVOIR is a single 20% bandwidth, SNR of 5, spectral resolution of 70, to determine the presence of water. Follow up spectral observations would be taken in 20% sub-bands in the visible and near-infrared up to a spectral resolution of 140 and an SNR of 8.5. The observing scenarios of the various HabEx architectures (coronagraph-only, starshade-only, and hybrid coronagraph with starshade) and the LUVOIR coronagraph are summarized in Table 2 of Morgan et al. 2021.³

An ideal observing scenario discovers and acquires spectra for as many Earth-like planets as possible with as few observations as possible. Determining the minimum number of observations needed to determine the planet's orbit is important to maximize the number of Earth-like spectra. Previous work⁴ has shown that, for a single planet with a circular orbit, three observations spanning more than half a period is the minimum number of observations to determine the semi-major axis and inclination to better than 10% error. Nielsen showed that four observations are the minimum for the general case, including highly eccentric systems (see Figure 3.1-2 of the HabEx Final Report¹). This observing requirement was added to the Exoplanet Open-Source Imaging Mission Simulator (EXOSIMS)⁵⁻¹⁵ yield simulation code and was used in the common comparison of HabEx and LUVOIR performed by the Exoplanet Exploration Program's Standard Definitions and Evaluation Team.^{16,17}

But what if multiple planets are discovered around a star? Does this change the heuristic of the minimum number of observations? Are additional observations needed in the effort to associate each dot in the image with the appropriate planet? What is the minimum required number and ideal cadence of observations to determine a planet's semi-major axis, inclination, and eccentricity to 10% error?

Determining which dots in the image belong to which planet could be performed with a brute force approach by inputting all permutations into an orbit fitting code, such as *orbitize!* which contains OFTI (Orbits for the Impatient), a Markov-chain Monte Carlo rejection sampler. Rejection sampling is a high fidelity solution that generates thousands to millions of simulated orbits that slowly converge to the best fit; it is best suited for a small number of planets or systems. A faster, more efficient tool is needed to perform a Monte Carlo study on thousands of systems to evaluate the impact of the number of observations and the cadence of observations, as well as the sensitivity to inclination, number of planets, and, though not covered in this paper, inner working angle (IWA), photometry, and utilizing null detections.

In this paper, we develop the framework and tools needed to perform a Monte Carlo study of thousands of systems. The first part of this framework is an algorithm to assign the positions of planets from multiple epochs to orbits. Section 2 discusses this algorithm as well as the sample synthetic planetary systems used and the simulation methods for the Monte Carlo studies. The initial results of validating and characterizing the performance of the deconfusion algorithm is presented in §3. The future work of improving both the deconfusion algorithm and our simulations, using our simulation framework to study the question of observation frequency and number, and further applications of this work are discussed in §4.

2. APPROACH

High contrast images of exoplanet systems are processed to determine the brightness and position of the exoplanet candidates relative to the host star, such as in the Roman CGI data challenge.¹⁸ The astrometric position measurements do not carry information regarding which detections correspond to which planets. If the number of possible orbits is greater than the number of possible planets (see Fig. 1), we run into a “confusion” problem.

We approach the confusion problem by a Monte-Carlo study of synthetic planetary systems. The goal is to assess the prevalence of cases in which it might be hard or impossible to determine which detection belongs to which planet. In §2.1 we describe an algorithm that assigns detections to orbits. The algorithm is used in the Monte-Carlo study to estimate the confusion rates for various parameters of planetary systems and observing schedules. The systems used in the study are described in §2.2 and the procedure that generates the synthetic detections is described in §2.3.

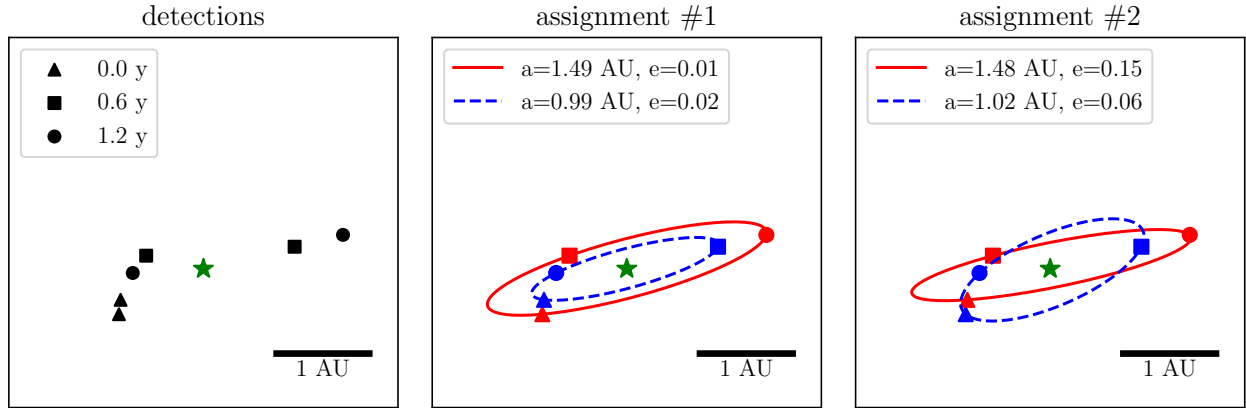


Figure 1. The confusion problem in planet assignment: several planets are detected at various positions and epochs (left) but which detection belongs to which planet is unknown. In some cases (center and right), detections can be assigned to different planets (e.g., the detection at 1.2 years marked by a circle). The resulting orbits are drastically different but “reasonable” for a solar-mass star in this example.

2.1 Deconfusion Algorithm

In this section we briefly describe the algorithm used for quick matching of astrometric data to orbits and orbits to planets (a full description is available in reference¹⁹). The first phase of the algorithm relies on fast and precise matching of 2D points to 3D Keplerian orbits. Unlike similar Monte-Carlo-based orbit-matching methods,^{20–22} our approach is semi-analytical and significantly faster, but is less accurate and does not currently provide error estimates. The second phase consists of identifying self-consistent *combinations* of orbits and ranking them based on how few planet groupings are used to describe the data.

2.1.1 Fast Orbit Matching

We assume astrometry consisting of Cartesian coordinates of planet candidates (“detections”) in the image plane as well as their corresponding epoch times. The mass of the star is assumed to be precisely known. The goal of orbit matching is to find all elliptical orbits with eccentricity below e_{max} that pass within distance Δr_{max} (or time Δt_{max}) of two or more detections.

In the first step, each pair and triplet of detections is matched with a Keplerian orbit. This is always possible since Keplerian orbits have six parameters and each detection provides two constraints on those parameters. Only orbits with eccentricity lower than e_{max} are kept at this step. This can significantly reduce the total number of orbits being analyzed.

In the second step, more detections are added to the orbits defined by the triplets of detections. We begin with an orbit that matches three detections and find a fourth observation that lies within Δr_{max} and Δt_{max} of the orbit. This procedure is repeated for all orbits that match three detections, then all orbits that match four detections, etc. The output of this step is a list of all orbits that match two or more detections.

2.1.2 Deconfusion

The list of all orbits that match two or more detections is likely to contain multiple orbits that match the same observations. Such orbits are mutually inconsistent since one detection should not be matched to multiple different planet groupings (ignoring the rare cases in which planets happen to align behind one another). In the deconfusion step, only combinations of orbits that do not share any detections are considered.

However, the number of self-consistent orbits is still large and some are clearly inferior to others. For example, it is possible to match an orbit to each detection (one possible combination) or an orbit to each detection pair

(an exponentially large number of possible combinations). Yet, more “reasonable” combinations should contain orbits that match a large number of detections.

The deconfuser simultaneously filters out inconsistent combinations of orbits and ranks them based on orbits that match the most detections. This is done by first selecting the orbits that match the most detections, then recursively proceeding with the remaining orbits and detections (excluding the ones matched to previously selected orbits). Orbits that match the second largest number of detections are considered next, and so on. Note that this approach may lead to multiple “highest ranking” combinations and may not include the combinations with the smallest number of planets. The development of other rankings and tie-breaking mechanisms are an item for future work.

2.2 Synthetic Planetary Systems

In order to investigate the nature of the confusion problem and assess our algorithm’s performance, we used a large set of synthetic planetary systems and simulated example scenarios with various system parameters and observing schedules. These synthetic systems were provided to us by Shannon Dulz who developed them for exoplanet radial velocity and direct imaging yield research.²³ The original set consists of 100,000 synthetic systems, and in our simulations so far we have used samples from the first 1500 of these systems. In each of the planetary systems, every planet has a defined mass and Keplerian elements, and every star has the same sun-like mass.

The occurrence rates that informed the joint mass and semi-major axis probability distribution in this set were sourced from Kepler mission data of planetary systems with F-, G-, and K- type stars.²³ The planet inclinations in each system were randomly sampled from a normal distribution with a mean of inclination of the system and with a standard deviation of three degrees.²⁴ The distribution of planet eccentricities in these systems was initially a beta distribution²⁵ which reflects statistics for largely single-exoplanet systems. However, planets in multiple-exoplanet systems have been shown to have less eccentric orbits, so we scaled the initial eccentricity distribution down by a factor of three in order to more accurately reflect known multiple-exoplanet system statistics.²⁶ The longitude of the ascending node, mean anomaly, and periastron angle were all randomly sampled from uniform distributions between zero and 2π . We note that in the field of radial velocity, it is common to fit planets sequentially, assuming no perceptible gravitational influence of the planets on one another. Given the small number of observations per star for direct imaging, the same assumption about no planet-to-planet orbit influences is adopted.

The systems were generated to be maximally packed with a majority of systems having between 25-40 planets, which is much higher than current estimates for exoplanet system demographics.²³ However, these systems were created to be dynamically stable, with adjacent planets all satisfying the stability criterion of having a mutual Hill radius less than nine using a circular orbit approximation.²³ More rigorous dynamic stability of sample systems is an item for future work. Since these systems had many more planets than were necessary for our purposes, we took random samples of seven planets from each of these systems and simulated multiple scenarios with between two and seven of those planets. Since we are particularly interested in studying the observation of systems with potentially Earth-like exoplanets, we ensured that one planet in each of our system samples was in the habitable zone of its sun-like star defined from 0.95 to 1.67 AU.¹⁶ Additionally, we excluded planets from our samples which had a semi-major axis less than 0.67 AU in order to narrow our study to planets with orbits at least 10% bigger than the HabEx IWA for a star at 10 parsecs. We also excluded planets with a semi-major axis greater than 10 AU.

2.3 Simulations

The format of the synthetic systems includes a list of keplerian elements for each planet in every system. We propagated the planet orbits to generate sample detections at multiple observation epochs, giving us simulated astrometric data showing where the planets would be located in simulated two dimensional images, as depicted in Fig. 1.

The coordinates of our sample detections in a 2D image plane along with their associated time stamps are then inputted to our deconfusion algorithm, which returns ranked sets of mutually consistent orbits to match detections to planets. The top ranked set describes the fewest number of planet groupings that can match all

of the input data. We simulate 1500 synthetic planetary systems in order to explore how often the algorithm returns the correct solution, and how often there are multiple top-ranked solutions that are tied. These tied spurious solutions are presently indistinguishable from the correct solution by our deconfusion algorithm, and future work will be required in order to rank them. A summary of our Monte Carlo study is described by the flow chart in Fig. 2.

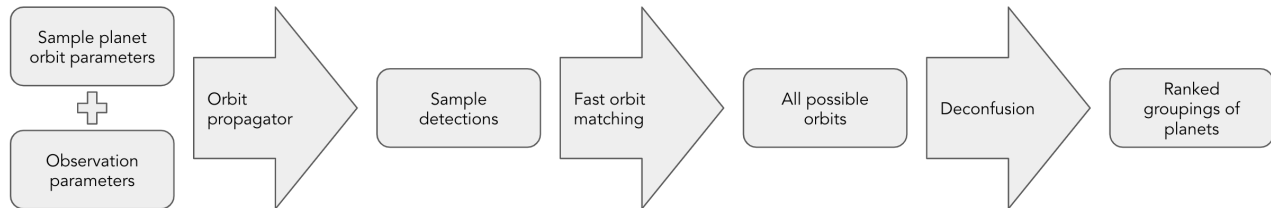


Figure 2. The flow chart describes the step by step process for the simulation of one sample system in our Monte Carlo study. Starting from the planet orbit parameters in each of our sample systems and observation scheduling parameters, we then propagate the orbits to obtain our sample detections. Those time-stamped detections then are fed into our deconfusion algorithm which ultimately returns the top candidate(s) for matching detections to planets.

In real direct imaging observations, there is non-trivial processing work to get from raw image data to the astrometric data we would input into our deconfusion algorithm.¹⁸ We have simplified this process for our purposes and simulated precise point-like planet detections without yet introducing astrometric uncertainty. The incorporation of this astrometry error into our sample detections is a goal for future work. Our deconfusion algorithm does, however, incorporate non-zero error tolerances Δr_{max} and Δt_{max} used to match additional points to orbits defined by groupings of planet detections, as described in §2.1.1. The HabEx 1σ astrometry error is expected to be 5 milliarcseconds (mas) due to the PSF size and a detection SNR of 5. In our simulations, we define these tolerances to allow detections to be matched to an orbit if the detections are located in the image with less than 10 mas (2σ expected HabEx astrometry error) displacement from the path of the orbit. At the present stage in our work, we use this 10 mas astrometry error tolerance to calculate a timing error parameter by approximating the time that the longest-period planets in our simulations would take to travel 10 mas in the 2D image plane for a face-on system. These simulation parameters are listed in Table 1. We use the parameter $e_{max} = 1$ in our deconfusion algorithm in order to avoid assumptions about prior eccentricity distributions.

We simulated the sample systems to be 10 parsecs away. To evaluate the effect of system inclination on our algorithm’s performance, we sampled detections from each of our sample systems multiple times over a range of orientations spanning from a “face-on” orientation (zero degree system inclination) to an “edge-on” orientation (90 degree inclination). These orientations are illustrated in Fig. 3 and the system inclination values used in our simulations are enumerated in Table 1. We also evaluated the effect of the number of planets, simulating between two and seven planets per system.

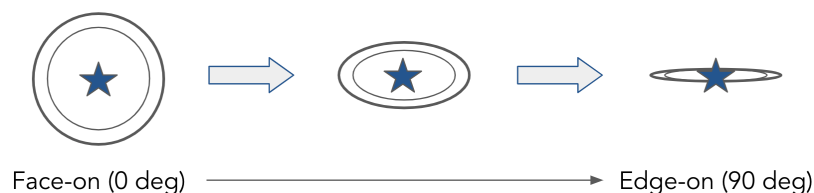


Figure 3. The value of inclination we define for each system refers to the angle of rotation around the horizontal axis from a “face-on” orientation at zero degrees to an “edge-on” orientation at 90 degrees.

We used two observing schedules in our simulations so far, as listed in Table 1. We sampled detections using three or four observation epochs evenly spaced over the period of one Earth year. An Earth year was used in

order to approximate the period of an Earth-like exoplanet in the habitable zone around a sun-like star.

Our simulations are simplified so that planets are visible for detection at all times. There are many reasons why some planets would not be visible in all direct imaging observations, including instrument IWA, planet size and contrast with host star, and planetary illumination phase. We aim to incorporate these factors into our simulations as part of our ongoing work, discussed in §4.

Table 1. For each unique combination of simulation parameters, 1500 sample systems are propagated, and their detections fed into the deconfusion algorithm. Parameters varied in these trials include number of planets and system inclination, and each of those simulations are repeated for both three and four evenly spaced observation epochs. The results are evaluated in §3 to determine in what cases the deconfusion algorithm is able to return the correct planet grouping solutions, as well as to determine when the correct solutions are identified exclusively without any spurious solutions with the same number of planet groupings.

Trials:	Simulation parameters:				
	Number of observations	Number of planets	System inclination [degrees]	Error tolerance Δr_{\max} [mas]	Error tolerance Δt_{\max} [years]
Number of observations	[3, 4]	3	0	10	0.05
Number of planets	[3, 4]	[2, 3, 4, 5, 6, 7]	0	10	0.05
System inclination	[3, 4]	3	[0, 20, 30, 45, 60, 80, 85, 90]	10	0.05

3. RESULTS

3.1 Number of Observations

For our first trial, we evaluated how our deconfusion algorithm performed with both three and four observation epochs in the generalized case of three planets in a face-on system. We generated sample detections for three and four observation epochs equally spaced over one Earth year for each of 1500 sample systems. The exact parameters used in this trial are listed in the first row of Table 1.

In the three epoch case, the deconfusion algorithm found the correct solution for 99.3% of systems. For 95.5% of systems the correct solution was identified exclusively, meaning there were no other spurious top-ranked solutions. In the four epoch case, the algorithm identified the correct solution for 100% of systems, and in 98.9% of systems the correct solution was identified exclusively.

In this trial, the algorithm was largely successful and there was only a small percentage of sample systems where further logic will need to be introduced in order to distinguish between the correct solution and other spurious solutions. Since our sample detections are “idealized” without any astrometry error, we expect the correct solution of planet groupings to be found by our algorithm every time, even if the algorithm cannot presently distinguish between the correct solution and other top-ranked tied spurious solutions. The few cases we found where the correct solution was not identified at all represent a numerical issue in the algorithm which we are currently working to remedy.

There is a significant difference between the cases of spurious solutions when there are three versus four observations of each planet. When there are three observations of each planet, there are often many combinations of three points that can form an ellipse around the host star. When there are four observations, the algorithm finds all triplets of points that form valid orbits, and then attempts to match a fourth point to the orbits defined by those triplets. The fourth point has to be within a defined margin of error in order to be considered close enough to the orbit to be considered a detection of the same planet. There is only a small likelihood that a

detection of one planet will fall close to the ellipse defined by three detections of a different planet. Therefore, we see significantly more spurious solutions in the three epoch case than the four epoch case. This difference becomes more apparent as we vary the system inclination and number of planets per system.

In addition to there being a higher percentage of systems where spurious solutions occurred in the three epoch case, there were often more spurious solutions per system, as seen in Fig. 4. In the four epoch case, the maximum number of spurious solutions for a given system was two, compared to the three epoch case where there were systems with up to 13 spurious solutions.

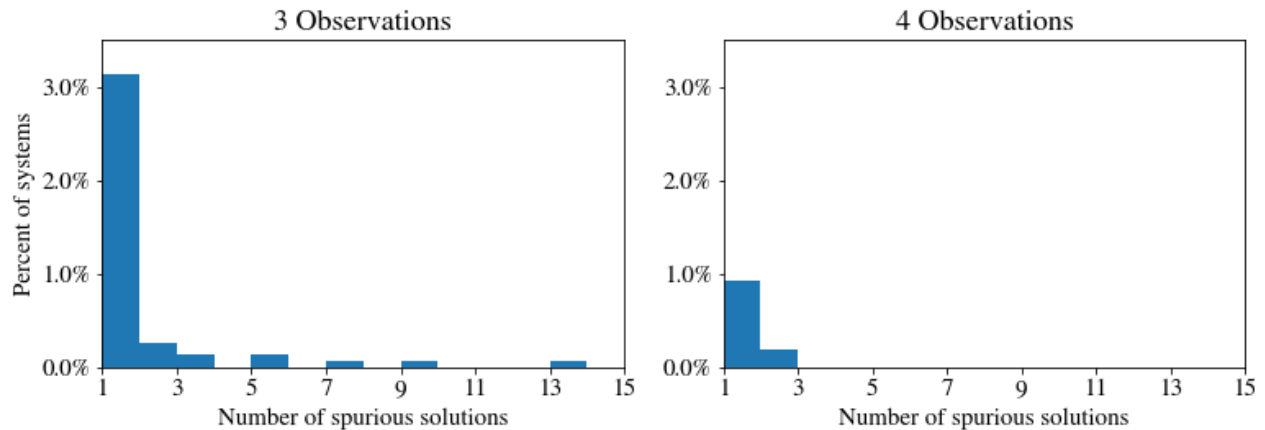


Figure 4. In the trial varying number of observations (as described by the first row of Table 1), 1500 face-on 3-planet systems were simulated and their sample detections were fed into the deconfusion algorithm for cases of three and four evenly spaced observation epochs. With three epochs, the deconfusion algorithm identified the correct solution exclusively with no spurious solutions 95.5% of the time, and 98.9% of the time in the four epoch case. These histograms describe the remaining cases where spurious incorrect solutions were identified which cannot yet be distinguished from the correct solution by the algorithm in its current state. Here we see that in the three epoch case, a higher percentage of sample systems returned spurious solutions, and the average number of spurious solutions found per system is higher than in the four epoch case. Note that in these histograms the bin for zero spurious solutions is not shown.

3.2 Number of Planets

We used the deconfusion algorithm to assess the spurious solution problem and its relationship to the number of planets in a system. As listed in the second row of Table 1, we simulated 1500 systems each with 2, 3, 4, 5, 6, and 7 planets. This was repeated for both three and four observation epochs.

The results presented in Fig. 5 show that the deconfusion algorithm identifies the correct solution in nearly all sample systems, but as we increase the number of planets per system, the prevalence of spurious solutions also increases. In the three observation case, as we go from two to seven planets, the percentage of systems where the correct solution was identified exclusively drops from 98.3% to 73.0%. It is worth noting that while the same trend occurred in the four observation case, it was to a lesser extent; the percentage of systems where the correct solution was identified exclusively only drops from 99.5% to 91.7%. The

The prevalence of spurious solutions when there are more planets highlights the need for future work to be done introducing additional logic into the algorithm to rank these tied spurious solutions. This will help us bridge the gap between the upper bound of how often the correct solution is identified at all (represented in Fig. 5 by the solid green lines) and the lower bound of how often the correct solution is identified exclusively (blue dotted lines).

3.3 System Inclination

Lastly, we used the deconfusion algorithm to assess the spurious solution problem as it relates to the inclination of the system relative to the observer. A graphic of how the system orientation changes from face-on at zero

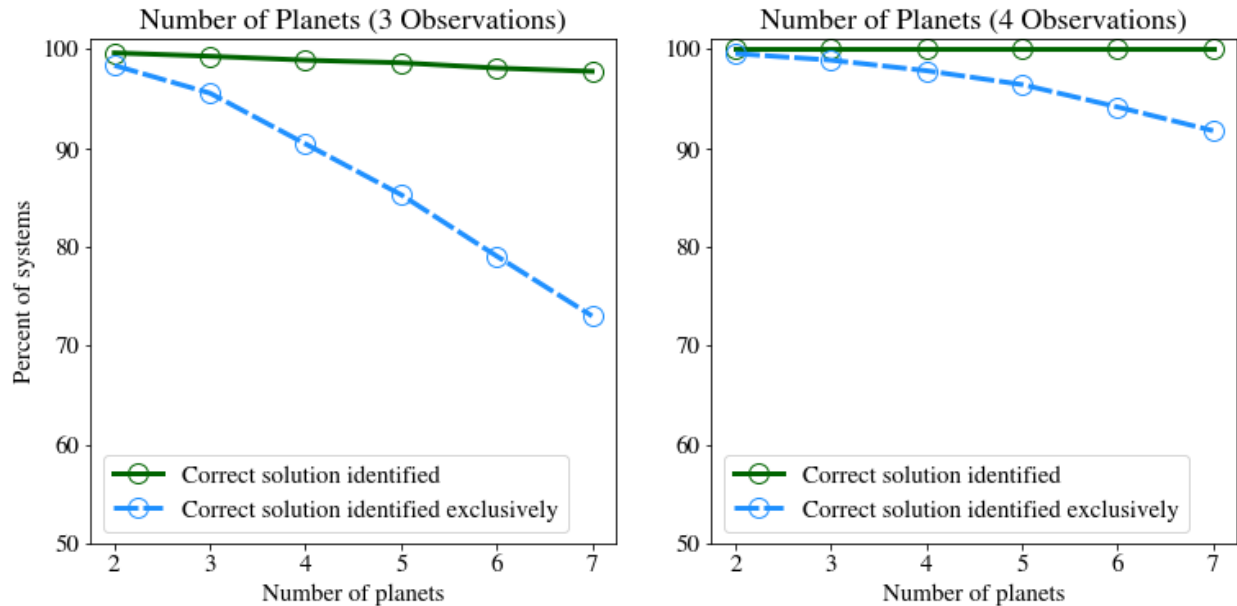


Figure 5. The trial varying number of planets per system is described in the second row of Table 1. The results are shown here for both the three and four observation cases. We see that the deconfusion algorithm is able to identify the correct solution nearly every time, but as we increase the number of planets, there are more systems with spurious incorrect solutions which cannot yet be distinguished from the correct solution with the algorithm's current logic. This trend is more significant with three observations than with four observations. The few systems in the three observation case where the algorithm did not find the correct solution at all represent a numerical issue in the algorithm which we are currently working to remedy.

degree inclination to edge-on at 90 degree inclination is presented in Fig. 3. We ran 1500 sample systems through the deconfusion algorithm for each value of system inclination, and repeated the experiment for three and four evenly spaced observation epochs. The simulation parameters for this trial varying system inclination are listed in the last row of Table 1, and the results are shown in Fig. 6.

For three observation epochs, the system inclination had a significant effect on the prevalence of spurious solutions, with the correct solution being identified exclusively in only 63.3% of nearly edge-on systems with 85 degree inclination. In the four observation case, the same trend was present but not to the same extent, with 76.7% of systems with 85 degree inclination where the correct solution was identified exclusively. While in the four observation case the correct solution was identified (even if not exclusively) for every single system, our algorithm did not find the correct solution in some of the higher inclination systems with only three epochs due to the aforementioned numerical issue in our algorithm that is in progress.

3.4 Summary

We presented an algorithm to match point sources of multi-planet systems taken at multiple epochs to planets. We also presented an approach to simulate a large number of multi-planet systems for Monte Carlo studies. We presented initial results for three and four evenly-spaced observations for a full range of inclination angles and for 2 to 7 planets in the system.

The simulations so far have shown us that the confusion problem for exoplanet direct imaging is significantly increased when more planets are present in an image, and when systems are inclined at a high angle relative to the observer. There is a higher rate of spurious solutions found which are not currently distinguished from the correct solution but that may be improved with additional logic. This situation is improved by having at least four detections of each planet in a system; in those cases, the correct solutions were identified exclusively at a higher rate with fewer spurious solutions.

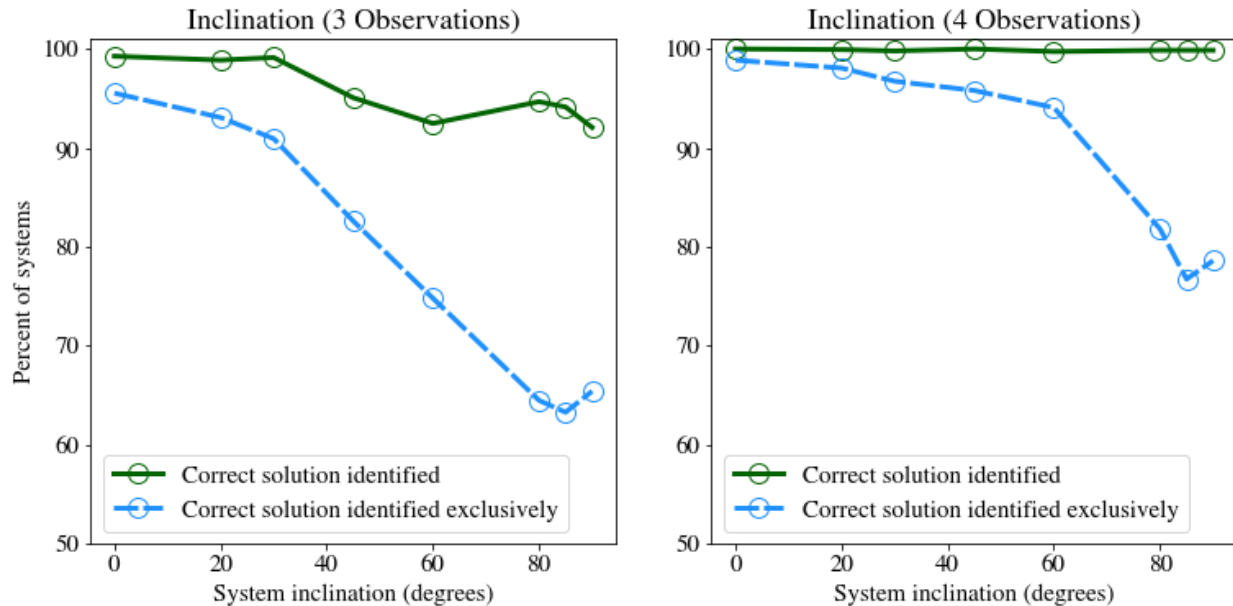


Figure 6. The trial varying system inclination is described in the last row of Table 1. Here results are shown for both three and four observations. The deconfusion algorithm is mostly able to identify the correct solution, but for higher inclination systems, we see a higher percentage of spurious incorrect solutions which cannot yet be distinguished from the correct solutions with the algorithm’s current logic. We find fewer spurious solutions when using four instead of three observations, but more work remains to enhance the deconfusion algorithm’s logic in order to close the gap between the dashed blue curve and the solid green curve. The few systems where the algorithm did not identify the correct solution at all represent a numerical issue in the algorithm which we are currently working to remedy.

In order to make concrete suggestions for observing strategies to mitigate the exoplanet confusion problem, we will need to enhance our simulations by “un-idealizing” our sample detections and introducing further tie-breaking methods into our deconfusion algorithm, as discussed in §4.

4. FUTURE WORK

To improve our understanding of the confusion problem and mitigate the issue of tied spurious solutions of planet groupings, we need to make improvements to our deconfusion tool. We are actively working on resolving minor numerical issues with the fast orbit matching step of our deconfusion algorithm so the correct solution can be found in all sample cases. Another improvement for our deconfusion tool is the implementation of metrics for distinguishing between top solutions which are currently tied in ranking because they contain the same number of planet groupings. Additional ranking metrics being considered include sorting based on lowest error for planet matching (when matching a fourth detection located within a defined error tolerance to an orbit defined by the first three detections), and other heuristics such as favoring planet groupings which more closely match known demographics for multiple-exoplanet systems such as low eccentricity and coplanarity of planet orbits.²⁷

We can also enhance our understanding of how the confusion problem impacts scientific applications by improving our sample systems and our simulation methods to more closely reflect realistic direct imaging conditions. For instance, we can make our sample detections less “idealized” by introducing astrometric error as well as including effects of planetary illumination phase, planet size and contrast with the host star, and instrument IWA, including utilizing null detections due to IWA obscuration. We also plan to introduce more rigorous metrics for dynamic stability in our sample systems.

These areas of improvement will enable us to build on our existing work and achieve our goal of using this algorithm to investigate optimal observing strategies for mitigating the exoplanet confusion problem, considering

both uniform and non-uniform observing cadences. The optimal observing strategy investigation will inform a heuristic for observing scenarios that can be used in potential future mission studies and can be incorporated into the EXOSIMS mission modeling code.

A further application of the deconfusion algorithm is direct incorporation into EXOSIMS for use during the dynamic observation-sequence simulation. The deconfusion algorithm provides a computationally fast approach for dynamic orbit determination that is tenable for thousands of Monte Carlo mission simulations. As the simulated mission progresses and each detection is made, the fast orbit matching algorithm can determine for each exosystem when sufficient observations have occurred, e.g. when a planet is known to be in the habitable zone or when all the discovered planets are known to be outside the habitable zone, and then the detection observations can be stopped and the spectral characterization observations begun.

The optimal observing strategies and heuristics gained from these applications of the deconfusion algorithm could lead to more effective observing schedules and potentially higher yields for potential future direct imaging missions that encounter multi-planet systems.

ACKNOWLEDGMENTS

We would like to thank Shannon Dulz for kindly providing us with a large set of maximally-packed, synthetic planetary systems, and Sarah Blunt for her input regarding the orbitize! python library for orbit fitting.

This research was carried out in part at the Massachusetts Institute of Technology (RSA No. 646345) and in part at the Jet Propulsion Laboratory, California Institute of Technology, under a contract with the National Aeronautics and Space Administration (80NM0018D0004) and funded through the Strategic University Research Partnership (SURP) program. ©2021. All rights reserved.

REFERENCES

- [1] Gaudi, B. S., Seager, S., Mennesson, B., Kiessling, A., Warfield, K., and the HabEx team, “The Habitable Exoplanet Observatory (HabEx) Mission Concept Study Final Report,” *arXiv e-prints*, arXiv:2001.06683 (Jan. 2020).
- [2] The LUVOIR Team, “The LUVOIR Mission Concept Study Final Report,” *arXiv e-prints*, arXiv:1912.06219 (Dec. 2019).
- [3] Morgan, R. M., Savransky, D., Turmon, M. J., Mennesson, B., Dula, W., Keithly, D. R., Mamajek, E. E., Newman, P., Plavchan, P., Robinson, T. D., Roudier, G., and Stark, C. C., “Faster Exo-Earth yield for HabEx and LUVOIR via extreme precision radial velocity prior knowledge,” *Journal of Astronomical Telescopes, Instruments, and Systems* **7**(2), 1 – 37 (2021).
- [4] Horning, A., Morgan, R., and Nielsen, E., “Minimum number of observations for exoplanet orbit determination,” in [*Techniques and Instrumentation for Detection of Exoplanets IX*], *Proc. SPIE* **11117**, International Society for Optics and Photonics (2019).
- [5] Savransky, D. and Kasdin, N. J., “Design reference mission construction for planet finders,” in [*Proc. SPIE*], **7010** (2008).
- [6] Savransky, D. and Kasdin, N. J., “Dynamic filtering for the analysis of astrometric and radial velocity data sets for the detection of exoplanets,” in [*AIAA Guidance, Navigation, and Control*], **6083** (2009).
- [7] Savransky, D. and Kasdin, N., “Automated design reference mission generation for theia,” in [*Bulletin of the American Astronomical Society*], **41**, 363 (2009).
- [8] Savransky, D., “Designing the next generation of extra-solar planet observatories,” in [*IPMJ Astrostats Meeting*], (2009).
- [9] Savransky, D., Kasdin, N., and Spergel, D., “Results from the automated design reference mission constructor for exoplanet imagers,” in [*Proc. SPIE*], **7440**, 744009–1 (2009).
- [10] Savransky, D., Kasdin, N. J., and Cady, E., “Analyzing the designs of planet finding missions,” *Publications of the Astronomical Society of the Pacific* **122**, 401–419 (Apr. 2010).
- [11] Savransky, D., Spergel, D. N., Kasdin, N. J., Cady, E. J., Lisman, P. D., Pravdo, S. H., Shaklan, S. B., and Fujii, Y., “Occulting ozone observatory science overview,” in [*Proc. SPIE*], **7731**, 77312H (2010).

- [12] Savransky, D., Delacroix, C., and Garrett, D., “EXOSIMS: Exoplanet Open-Source Imaging Mission Simulator.” Astrophysics Source Code Library (June 2017).
- [13] Savransky, D. and Garrett, D., “WFIRST-AFTA coronagraph science yield modeling with EXOSIMS,” *Journal of Astronomical Telescopes, Instruments, and Systems* **2**(1), 011006 (2015).
- [14] Delacroix, C., Savransky, D., Garrett, D., Lowrance, P., and Morgan, R., “Science yield modeling with the Exoplanet Open-Source Imaging Mission Simulator (EXOSIMS),” in [*Proc. SPIE*], **9911**, 991119–991119–10 (2016).
- [15] Savransky, D. and the EXOSIMS team, “Exoplanet open-source imaging mission simulator.” <https://github.com/dsavransky/EXOSIMS> (2020).
- [16] Morgan, R., Savransky, D., Stark, C., and Nielsen, E., “The standard definitions and evaluation team final report: A common comparison of exoplanet yield.” https://exoplanets.nasa.gov/system/internal_resources/details/original/1434_Standards_Team_Final_Report_20191007.pdf (2019).
- [17] Morgan, R., Savransky, D., Turmon, M., Mennesson, B., Mamajek, E., Shaklan, S., Soto, G., Stapelfeldt, K., Dula, W., and Keithly, D., “Standard exoplanet yield evaluation for the LUVOIR and HabEx concept studies,” in [*Techniques and Instrumentation for Detection of Exoplanets IX*], Shaklan, S. B., ed., **11117**, 1 – 20, International Society for Optics and Photonics, SPIE (2019).
- [18] Girard, J. H., Bogat, E., Gonzalez-Quiles, J., Hildebrandt, S. R., Kane, S. R., Li, Z., Turnbull, M. C., Stark, C., Mandell, A., Meshkat, T., and Zimmerman, N. T., “The Roman exoplanet imaging data challenge: a major community engagement effort,” in [*Space Telescopes and Instrumentation 2020: Optical, Infrared, and Millimeter Wave*], Lystrup, M., Perrin, M. D., Batalha, N., Siegler, N., and Tong, E. C., eds., *Proc. SPIE* **11443**, 596 – 605, International Society for Optics and Photonics, SPIE (2020).
- [19] Pogorelyuk, L. et al., “Detection confusion in multi-exoplanet direct images,” in preparation.
- [20] Wertz, O., Absil, O., González, C. A. G., Milli, J., Girard, J. H., Mawet, D., and Pueyo, L., “VLT/SPHERE robust astrometry of the HR8799 planets at milliarcsecond-level accuracy,” *Astronomy & Astrophysics* **598**, A83 (Feb. 2017).
- [21] Mede, K. and Brandt, T. D., “The exoplanet simple orbit fitting toolbox (ExoSOFT): An open-source tool for efficient fitting of astrometric and radial velocity data,” *The Astronomical Journal* **153**, 135 (Mar. 2017).
- [22] Blunt, S., Wang, J. J., Angelo, I., Ngo, H., Cody, D., Rosa, R. J. D., Graham, J. R., Hirsch, L., Nagpal, V., Nielsen, E. L., Pearce, L., Rice, M., and Tejada, R., “orbitize!: A comprehensive orbit-fitting software package for the high-contrast imaging community,” *The Astronomical Journal* **159**, 89 (Feb. 2020).
- [23] Dulz, S. D., Plavchan, P., Crepp, J. R., Stark, C., Morgan, R., Kane, S. R., Newman, P., Matzko, W., and Mulders, G. D., “Joint radial velocity and direct imaging planet yield calculations. i. self-consistent planet populations,” *The Astrophysical Journal* **893**, 122 (apr 2020).
- [24] Fang, J. and Margot, J.-L., “Architecture of Planetary Systems Based on Kepler Data: Number of Planets and Coplanarity,” *The Astrophysical Journal* **761**, 92 (Dec. 2012).
- [25] Kipping, D. M., “Parametrizing the exoplanet eccentricity distribution with the beta distribution,” *Monthly Notices of the Royal Astronomical Society* **434**, L51–L55 (July 2013).
- [26] Limbach, M. A. and Turner, E. L., “Exoplanet orbital eccentricity: Multiplicity relation and the solar system,” *Proceedings of the National Academy of Sciences* **112**(1), 20–24 (2015).
- [27] Xie, J.-W., Dong, S., Zhu, Z., Huber, D., Zheng, Z., De Cat, P., Fu, J., Liu, H.-G., Luo, A., Wu, Y., Zhang, H., Zhang, H., Zhou, J.-L., Cao, Z., Hou, Y., Wang, Y., and Zhang, Y., “Exoplanet orbital eccentricities derived from lamost-kepler analysis,” *Proceedings of the National Academy of Sciences* **113**(41), 11431–11435 (2016).